Molecular Photonics

Lecture 9

QD/imaging

Semiconductor NPs

Quantum dots

Quantum confinement

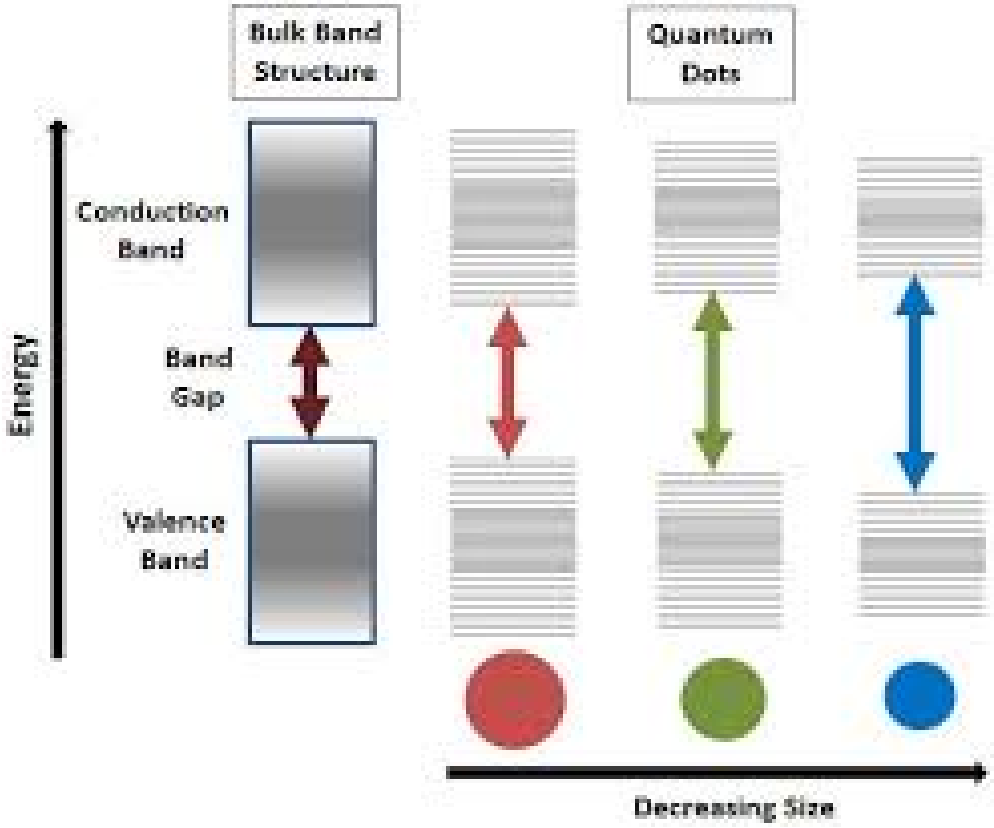

http://www.youtube.com/watch?v=B195U--HI8A

Size dependent absorption and emission

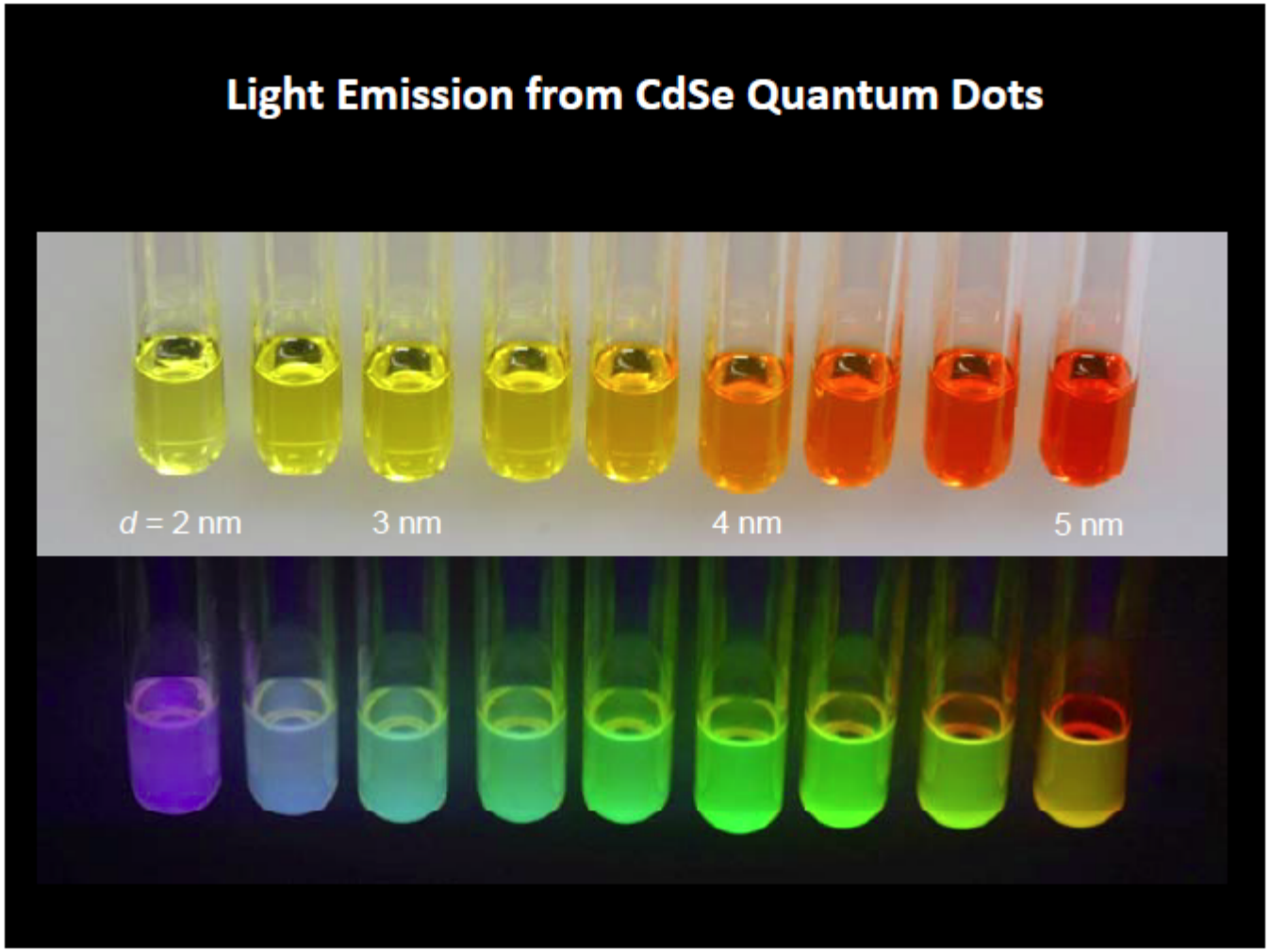

From atom to bulk

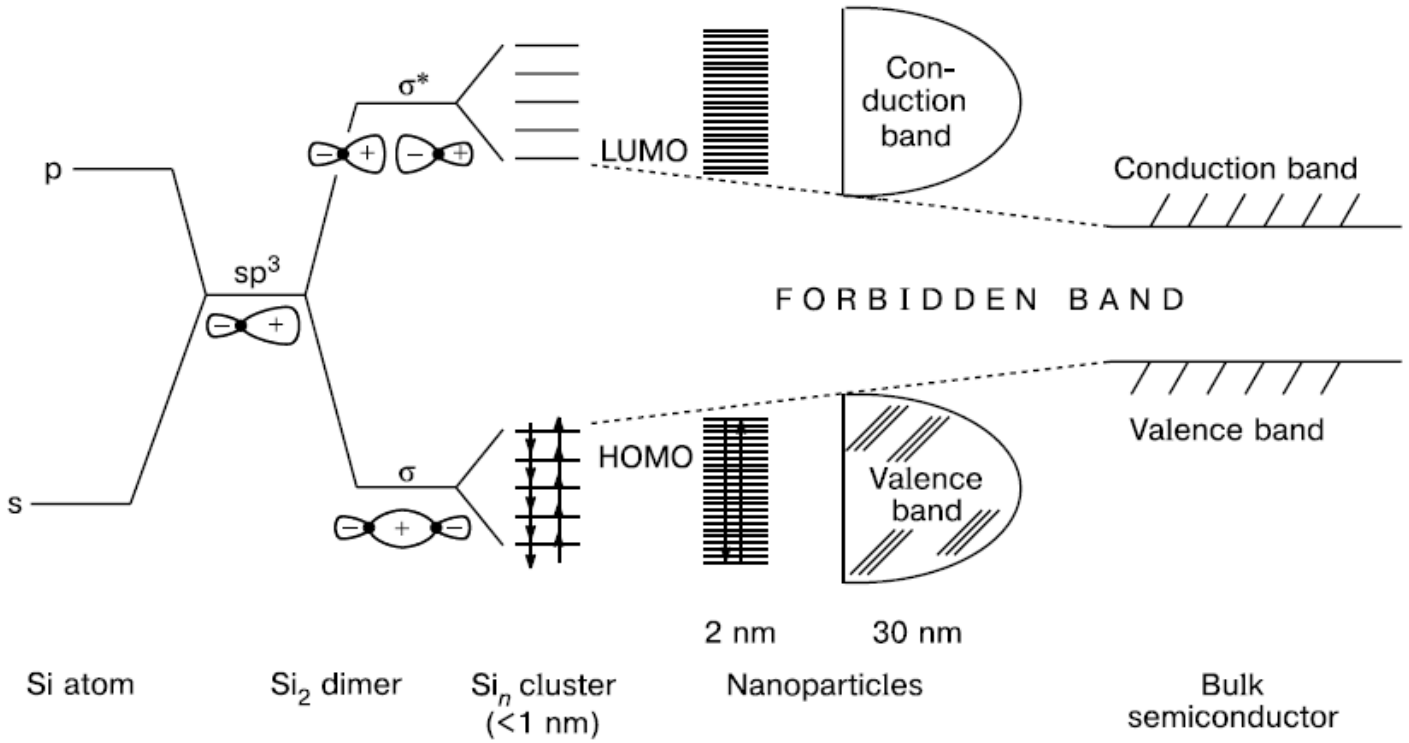

Bohr Radius

*The **Bohr radius** (1913) is the most probable distance between the proton and electron in a hydrogen atom in its ground state*

Niels Henrik David Bohr
(Nicholas Baker)

$$a_0 = \frac{4\pi\varepsilon_0\hbar^2}{m_e e^2} = 0.529 \text{ Å}$$

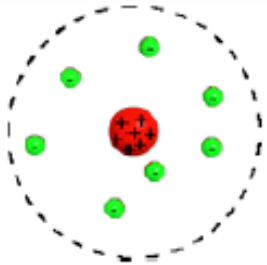

The Rutherford model or planetary model

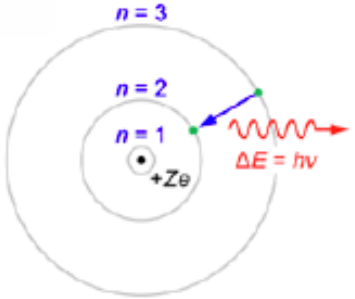

The Bohr-Rutherford model

Slides from

The University of Tokushima
6/25/2012

Vasudevanpillai Biju

Definition of Exciton/ Bohr Exciton Radius

- The optical properties of a material are usually determined by electronic transitions within the material and light scattering effects. Due to Coulomb interaction, the electrons and holes existing in a material are known to form excitons. Therefore, the optical nature of semiconductors can be understood by investigating the properties of the excitons.
- An exciton is composed of an electron and a hole. The distance between the electron and the hole within an exciton is called Bohr radius of the exciton. Typical exciton Bohr radius of semiconductors is of a few nanometers. In bulk semiconductors, the exciton can move freely in all directions. When the length of a semiconductor is reduced to the same order as the exciton radius, i.e., to a few nanometers, quantum confinement effect occurs and the exciton properties are modified. Depending on the dimension of the confinement, three kinds of confined structures are defined: quantum well (sometimes termed QW), quantum wire (QWR) and quantum dot (QD). In a QW, the material size is reduced only in one direction and the exciton can move freely in other two directions. In a QWR, the material size is reduced in two directions and the exciton can move freely in one direction only. In a QD, the material size is reduced in all directions and the exciton can not move freely in any direction.
- In these confined structures, the exciton nature is modified and novel optical properties are expected. As a result, these structures are good candidates for developing high-performance optoelectronic devices such as semiconductor light-emitting diodes and laser diodes.

The electron in the conduction band and the hole in the valence band can be held together by the electrostatic attraction, to form exciton. The interaction between electron and hole can be described by a hydrogen-like Hamiltonian (cgs units)

$$\hat{H} = -\frac{\hbar^2}{2M}\nabla_e^2 - \frac{\hbar^2}{2\mu}\nabla_h^2 - \frac{e^2}{\varepsilon\,|\,r_e - r_h\,|} \qquad (1)$$

where the M is the total mass $M = m_e^* + m_h^*$ and μ is the reduced mass $\mu = m_e^* m_h^* / (m_e^* + m_h^*)$; m_e^* and m_h^* are the effective masses of the electron and hole, respectively.

The band gap (the minimum energy necessary to excite an electron from the valence level to the conduction level) of semiconductor nanocrystals (quantum dots) is given by

$$E_{g,QD} = E_{g,bulk} + \frac{\hbar^2 \pi^2}{2\mu r^2}. \qquad (7)$$

where the second term describes the energy levels of a particle of mass μ in a spherically symmetric potential box.

Above equation explains qualitatively well the quantum size effects in quantum dots: the increase of interband energy separation with the decrease of quantum dot size.

In fact, a more accurate equation for the calculation of exciton energy in semiconductor nanocrystals can be derived as

$$E_{g,QD} = E_{g,bulk} + \frac{\hbar^2 \pi^2}{2\mu r^2} - \frac{1.786 e^2}{\varepsilon_r \varepsilon_0 r} - 0.248 \frac{\mu e^4}{2\hbar^2 \varepsilon_r^2 \varepsilon_0^2}. \qquad (8)$$

Exciton Bohr Radius and Quantum Confinement

Excitons are coupled electron-hole pairs via Coulomb attraction

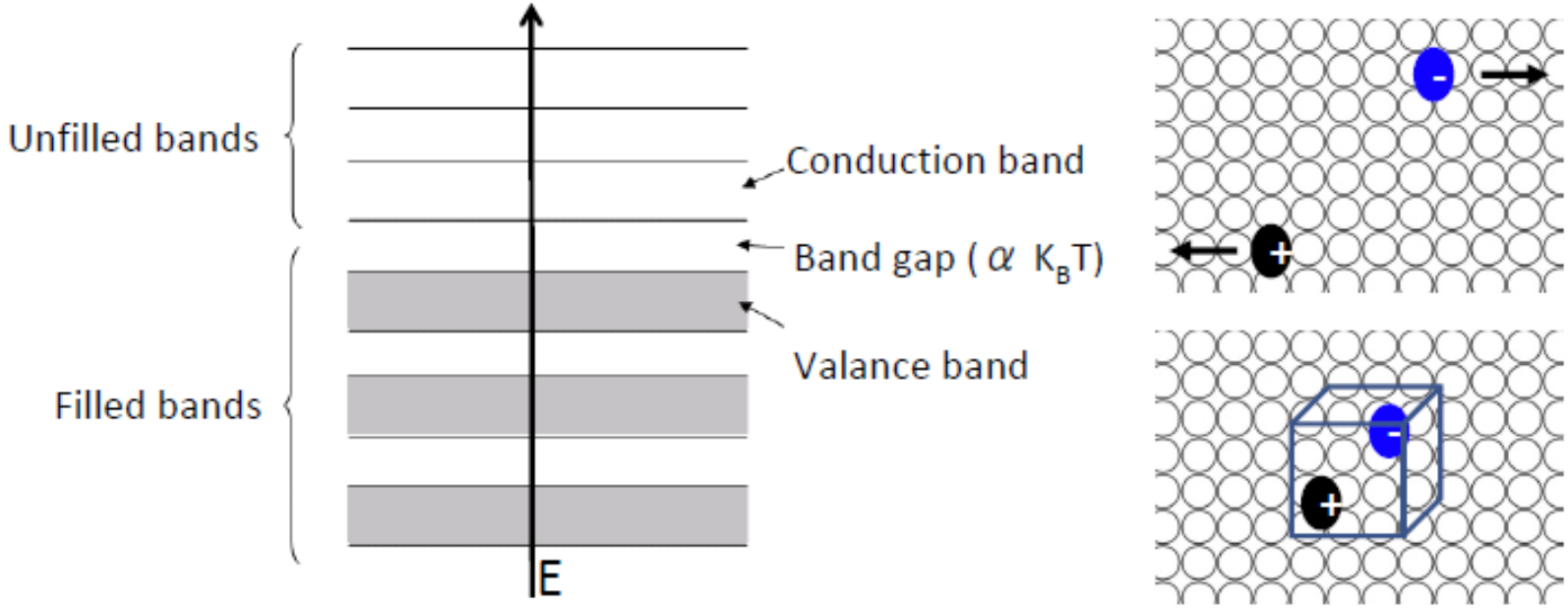

In bulk semiconductors, the exciton can move freely in all directions. When the length of a semiconductor is reduced to the same order as the exciton radius, i.e., to a few nanometers, quantum confinement effect occurs and the exciton properties are modified. Depending on the dimension of the confinement, three kinds of confined structures are defined: quantum well (QW), quantum wire (QR) and quantum dot (QD)

Exciton Bohr Radius and Quantum Confinement

Bohr Radius $$a_0 = \frac{4\pi\varepsilon_0\hbar^2}{m_e e^2} = 0.529 \text{ Å}$$

Exciton Bohr Radius $$a_{\text{exciton}} = \frac{a_0 \varepsilon}{m^* / m_e}$$

E.g., Silicon

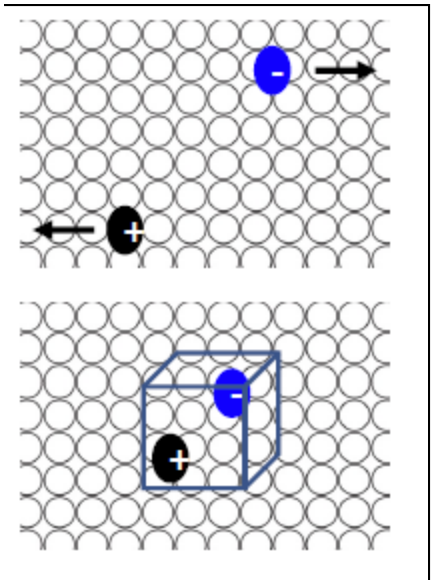

$$\varepsilon = 11.9;\ m_e^* = 0.26\ m_e,\ m_h^* = 0.36\ m_e$$

$$\Rightarrow m^* = \frac{m_e^* \cdot m_h^*}{m_e^* + m_h^*} m_e = 0.15 m_e$$

$$\Rightarrow a_{\text{exciton}} = \frac{a_0 \cdot 11.9}{0.15} = 79.3 a_0 = 4.2 \text{ nm}$$

Quantum Dots

Quantum Dots are tiny semiconductor nanoparticles in zero dimension in which holes and electrons are three directionally confined

Size of quantum dots: 2-10 nm in diameter (10~50 atoms long)

Quantum dots show properties similar to atoms/molecules than bulk
Thus, they are nicknamed artificial atoms

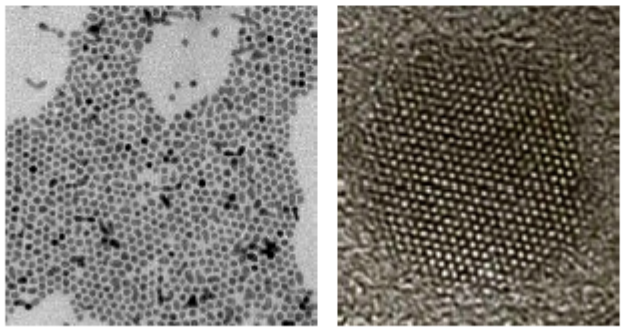

CdSe Quantum Dots

Table 1. Calculated exciton Bohr radii for various semiconductor quantum dots as a function of effective mass and dielectric constant based on Eq. 4.

Quantum Dot Semiconductor type	m^*_e Electron effective mass	m^*_h Hole Effective mass	Reduced mass μ	ε_r Dielectric constant relative to vacuum	α(Å)
CdSe	0.13	0.45	0.108	10.1	61
CdS	0.21	0.68	0.16	9.4	34
ZnS	0.34	1.76	0.29	8.9	18
GaAs	0.067	0.082	0.036	13.2	216
InSb	0.014	0.42	0.013	17.3	785

Band Gap Structure in Cadmium Selenide Quantum Dots

Carrier recombination processes in a quantum dot

- Radiative relaxation at the band edge
- Phonon-assisted non-radiative relaxation
- Nonradiative Auger relaxation
- Radiative and non-radiative relaxations at the surface defects

Photoluminescence in a CdSe quantum dot

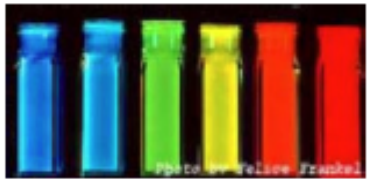

(i) Recombination at the band edge (transitions from the lowest unoccupied state, which is a combination of the 5s orbitals of cadmium, to the highest occupied state, which is a combination of the 4p orbitals of selenium)

(ii) Deactivation of excited electrons (holes) at the surface states

Band Gap Structure in CdSe Quantum Dots

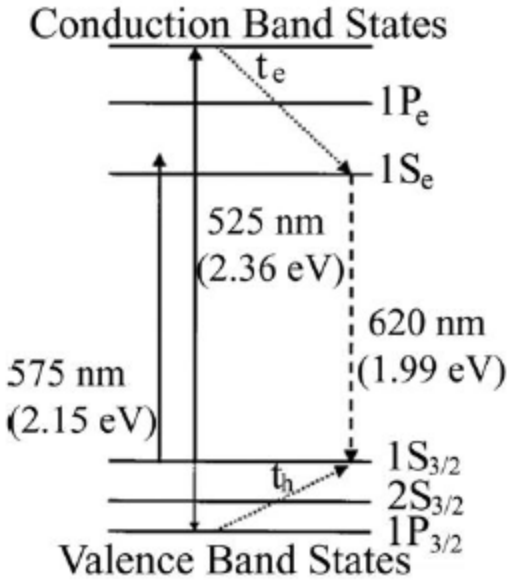

Real Life

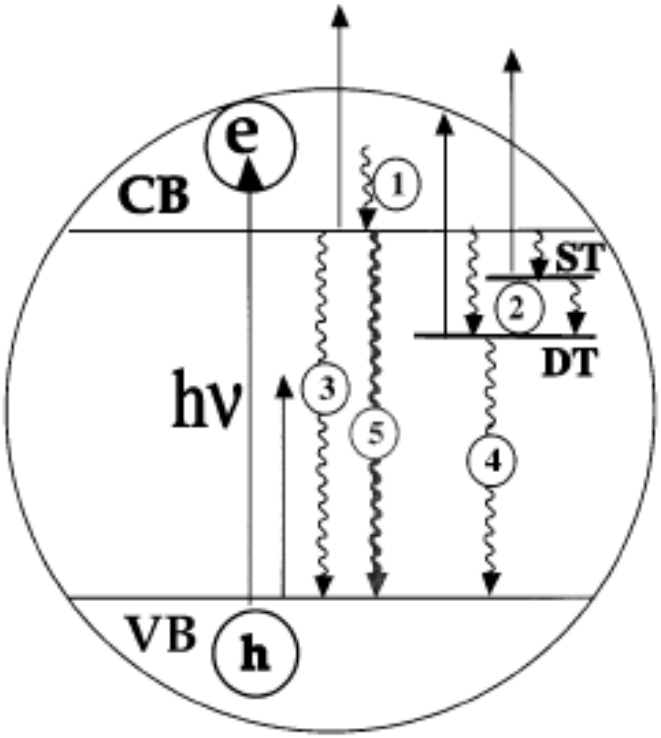

Figure 4. Schematic illustration of charge carrier relaxation in semiconductor NPs and the pump–probe scheme for monitoring the carrier dynamics. The long solid line with upward arrow indicates excitation and the short solid lines with upward arrows indicate probe of the conduction band, shallow and deep trap states, and valence band, respectively. The curved lines with downward arrows indicate different relaxation processes: (1) electronic relaxation within the conduction band, (2) trapping into shallow trap (ST) and deep trap (DT) states and further trapping from ST to DP, (3) bandedge electron–hole recombination, (4) trapped electron–hole recombination, and (5) exciton–exciton annihilation.

Type I and II

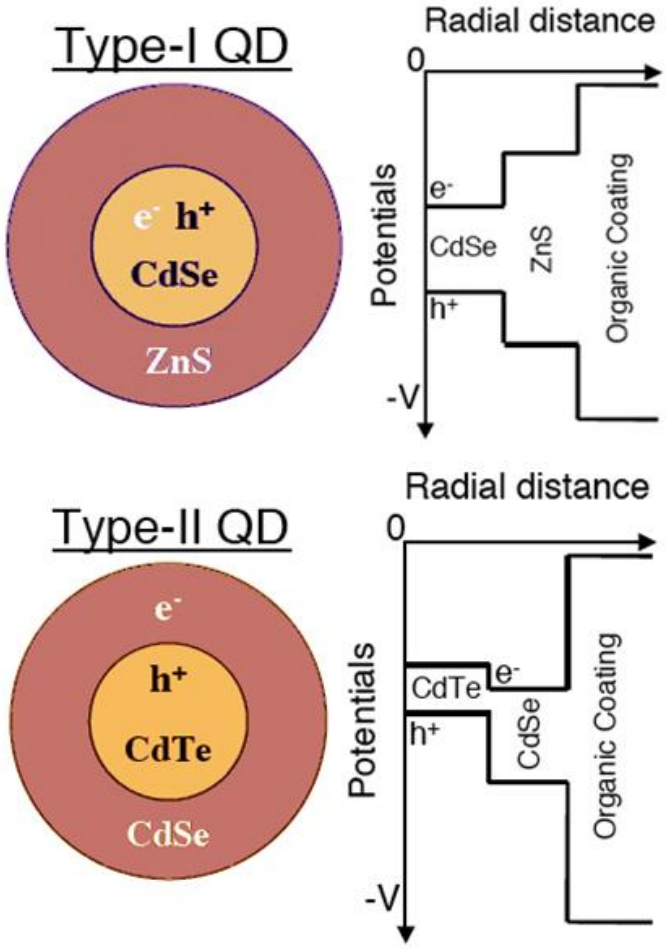

Type-I vs. Type-II Quantum Dots. In Type-I QDs, all charge carriers are confined in the core material in which radiative recombination occurs. In Type-II QDs, charge carriers are segregated in the core and shell; radiative recombination occurs across the material interface

The core and the shell are typically composed of type II–VI, IV–VI, and III–V semiconductors, with configurations such as CdS/ZnS, CdSe/ZnS, CdSe/CdS, and InAs/CdSe (typical notation is: core/shell

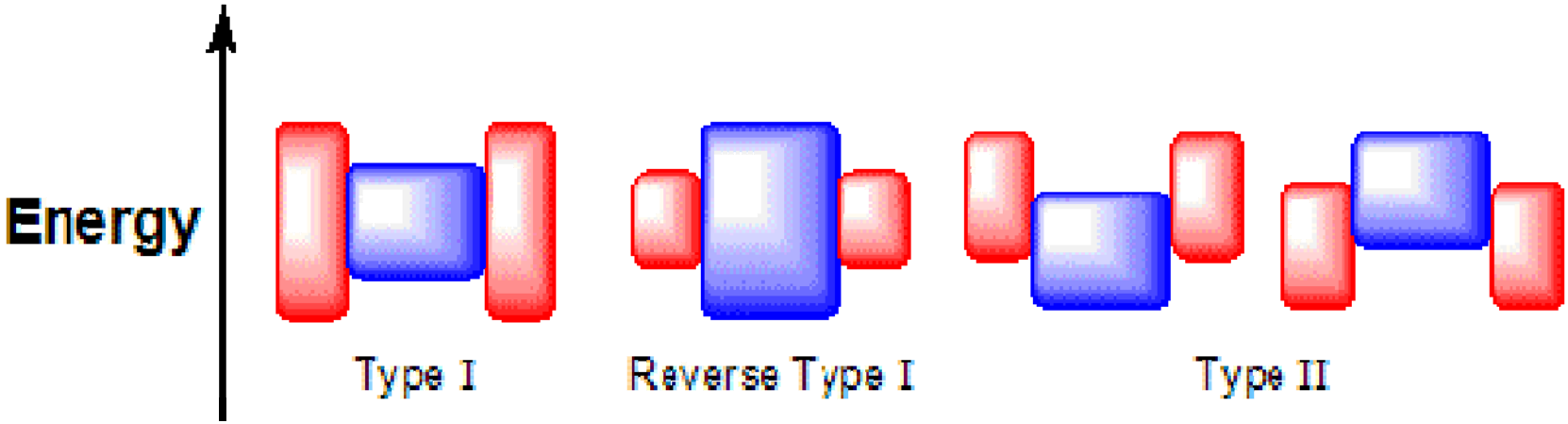

In a Type I CSSNC, the bandgap of core is smaller than that of the shell. Both the conduction and valence band edges of the core lie within the bandgap of the shell, which confines both electrons and holes in the core.

Examples
CdSe/CdS, CdSe/ZnS,and InAs/CdSe

In the type II configuration, the valence and conduction band edge are both lower or higher than the band edges of the shell.

Examples
ZnTe/CdSe, CdTe/CdSe, CdS/ZnSe

Type I and II

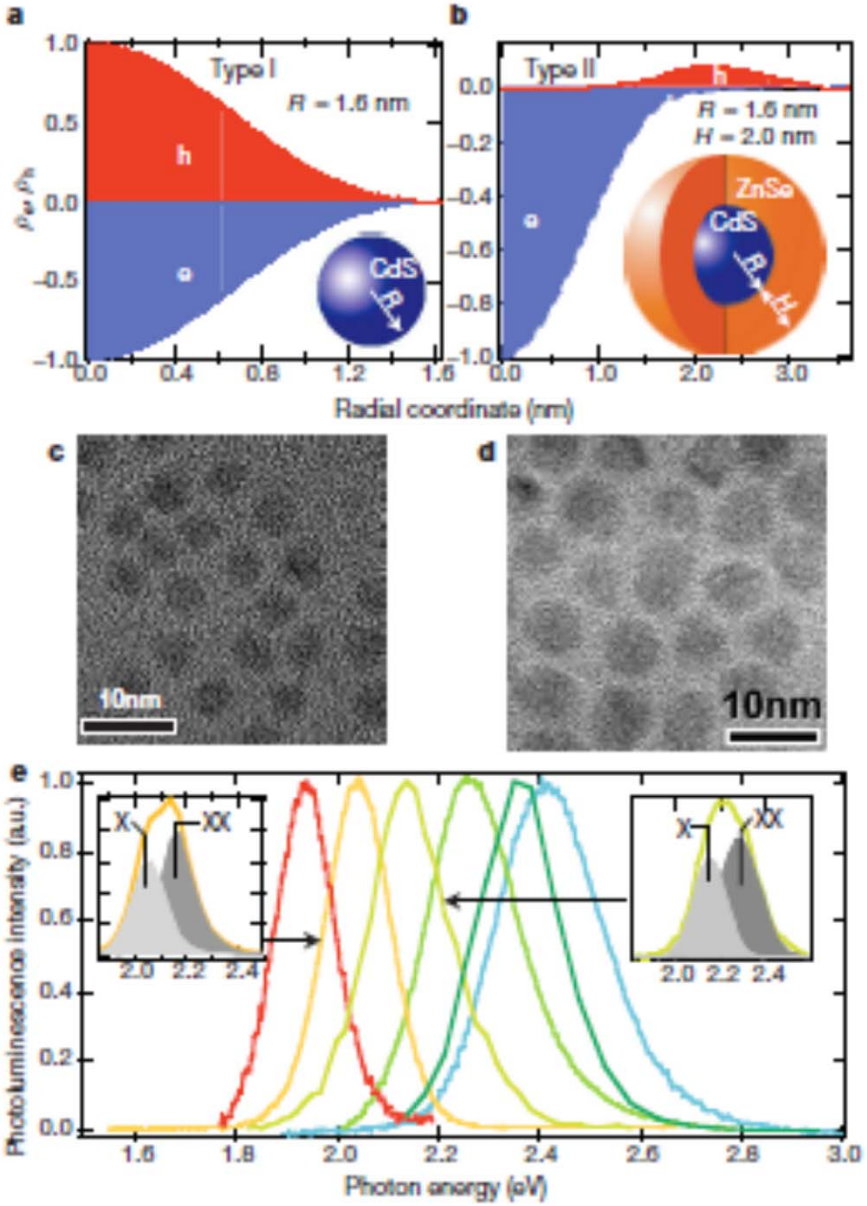

Vol 447|24 May 2007|doi:10.1038/nature05839 nature

ARTICLES

Single-exciton optical gain in semiconductor nanocrystals

Victor I. Klimov[1], Sergei A. Ivanov[1], Jagjit Nanda[1], Marc Achermann[1], Ilya Bezel[1], John A. McGuire[1] & Andrei Piryatinski[1]

Figure 2 | Type-I CdS NCs and type-II CdS/ZnSe core/shell heteronanostructures. **a**, Spatial distributions of electron (ρ_e) and hole (ρ_h) charge densities are nearly identical in type-I NCs (inset) (calculated for $R = 1.6$ nm). **b**, In type-II core/shell NCs (inset), electrons are primarily localized in the core, while holes reside in the shell, which leads to a significant difference in radial distributions of ρ_e and ρ_h (calculated for $R = 1.6$ nm and $H = 2$ nm). **c**, A transmission electron microscopy (TEM) image of a core CdS particle of ~2.4 nm radius. **d**, TEM images of hetero-NCs fabricated using the cores shown in **c**. The core/shell NC radius is ~3.4 nm, indicating that the shell width is ~1.0 nm. Because of the small difference between electron scattering cross-sections of CdS and ZnSe, the CdS/ZnSe interface is not discernable in the TEM image. **e**, Emission spectra of a series of CdS/ZnSe core/shell NCs synthesized using CdS cores with radii of 1.6 nm (higher-energy emission) and 2.6 nm (lower-energy emission) and various shell widths. Insets, early-time emission spectra measured at high pump intensities can be deconvolved into the single-exciton (X) and the biexciton (XX) bands. The spacing between these two bands indicates giant X–X interaction energies of more than 100 meV. a.u., arbitrary units.

Quantum Dots for Live Cells, in Vivo Imaging, and Diagnostics

X. Michalet,[1*] F. F. Pinaud,[1*] L. A. Bentolila,[1] J. M. Tsay,[1] S. Doose,[1†] J. J. Li,[1] G. Sundaresan,[2] A. M. Wu,[2] S. S. Gambhir,[2,4] S. Weiss[1,3*]

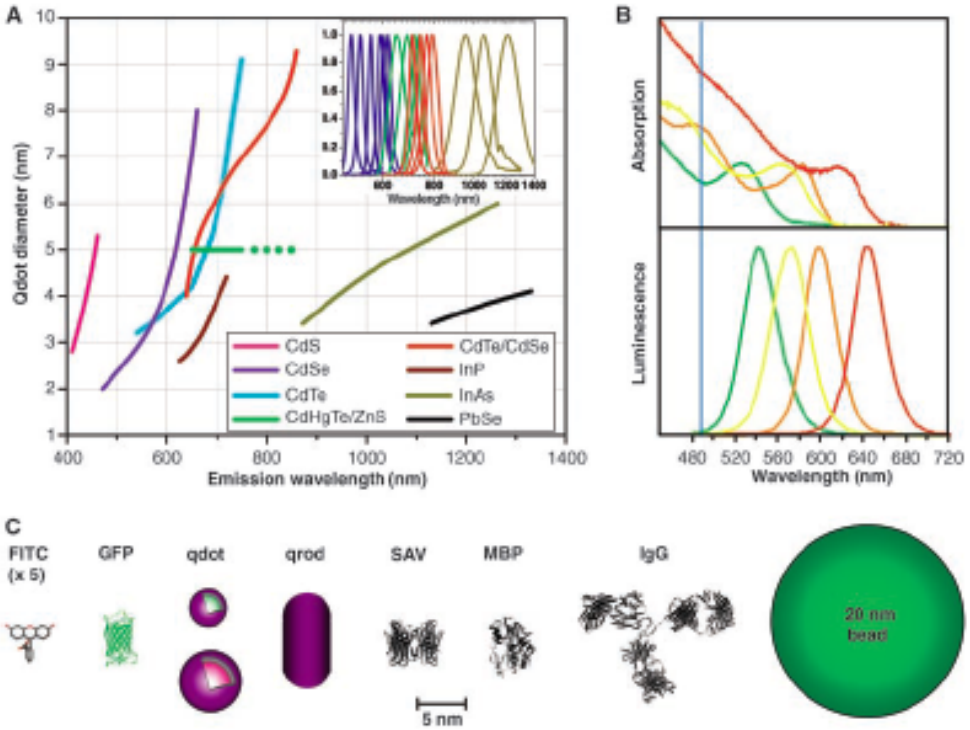

Fig. 1. (A) Emission maxima and sizes of quantum dots of different composition. Quantum dots can be synthesized from various types of semiconductor materials (II-VI: CdS, CdSe, CdTe…; III-V: InP, InAs…; IV-VI: PbSe…) characterized by different bulk band gap energies. The curves represent experimental data from the literature on the dependence of peak emission wavelength on qdot diameter. The range of emission wavelength is 400 to 1350 nm, with size varying from 2 to 9.5 nm (organic passivation/solubilization layer not included). All spectra are typically around 30 to 50 nm (full width at half maximum). Inset: Representative emission spectra for some materials. Data are from (*12*, *18*, *27*, *76*–*82*). Data for CdHgTe/ZnS have been extrapolated to the maximum emission wavelength obtained in our group. (B) Absorption (upper curves) and emission (lower curves) spectra of four CdSe/ZnS qdot samples. The blue vertical line indicates the 488-nm line of an argon-ion laser, which can be used to efficiently excite all four types of qdots simultaneously. [Adapted from (*28*)] (C) Size comparison of qdots and comparable objects. FITC, fluorescein isothiocyanate; GFP, green fluorescent protein; qdot, green (4 nm, top) and red (6.5 nm, bottom) CdSe/ZnS qdot; qrod, rod-shaped qdot (size from Quantum Dot Corp.'s Web site). Three proteins—streptavidin (SAV), maltose binding protein (MBP), and immunoglobulin G (IgG)—have been used for further functionalization of qdots (see text) and add to the final size of the qdot, in conjunction with the solubilization chemistry (Fig. 2).

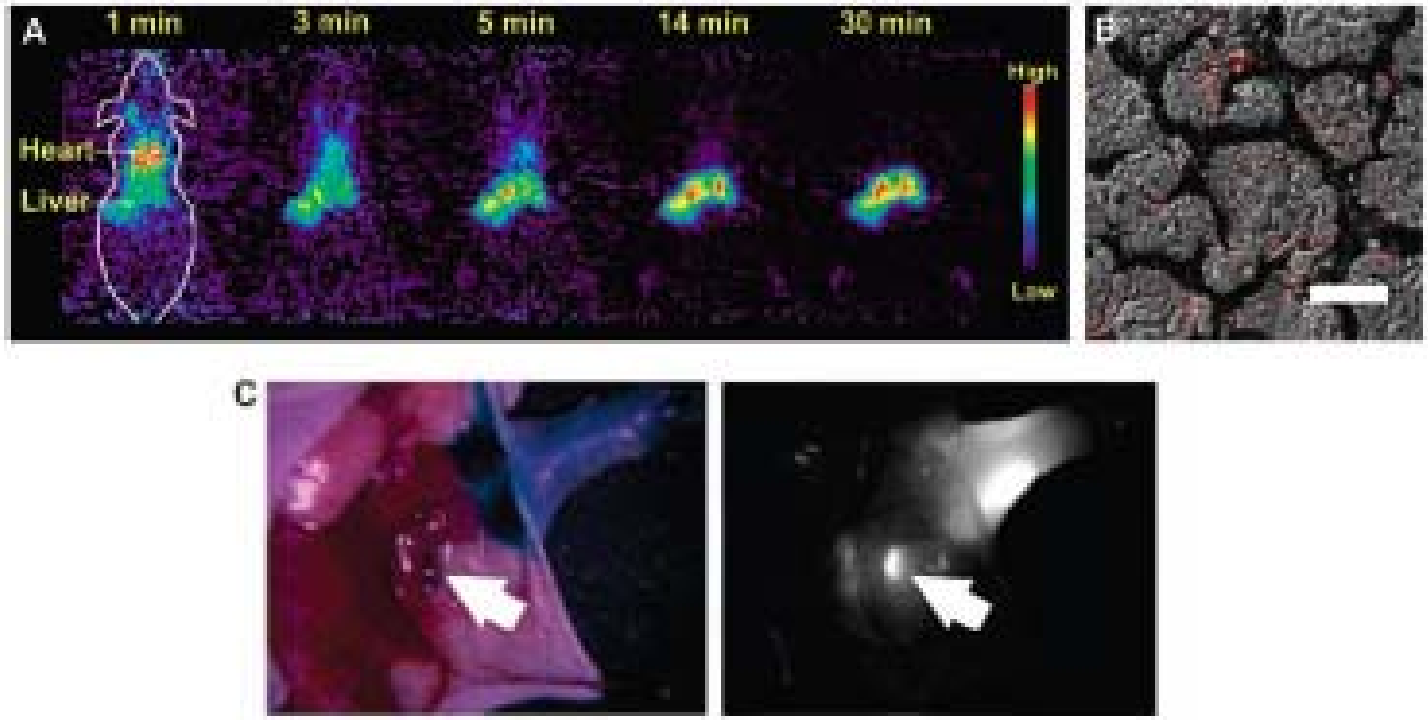

Fig. 4. Animal use of qdots. (A and B) microPET and fluorescence imaging of qdots. Qdots having DOTA (a chelator used for radiolabeling) and 600-dalton PEG on their surface were radiolabeled with ^{64}Cu (positron-emitting isotope with half-life of 12.7 hours). These qdots were then injected via the tail vein into nude mice (~80 μCi per animal) and imaged in a small animal scanner. (A) Rapid and marked accumulation of qdots in the liver quickly follows their intravenous injection in normal adult nude mice. This could be avoided by functionalizing qdots with higher molecular weight PEG chains, as other studies have shown (49). (B) Overlay of DIC and fluorescence images of hepatocytes from a mouse shows the accumulation of qdots within liver cells. Scale bar, 20 μm. A further step could involve TEM imaging of the precise localization of qdots in cells, illustrating the potential of qdots as probes at the macro-, micro-, and nanoscales. (C) Surgical use of NIR qdots. A mouse was injected intradermally with 10 pmol of NIR qdots in the left paw, 5 min after reinjection with 1% isosulfan blue and exposure of the actual sentinel lymph node. Left, color video; right, NIR fluorescence image. Isosulfan blue and NIR qdots were localized in the same lymph node (arrows). Copyright 2004 Nature Publishing Group. Reproduced with permission from (60).

Imaging

Fluorescent imaging

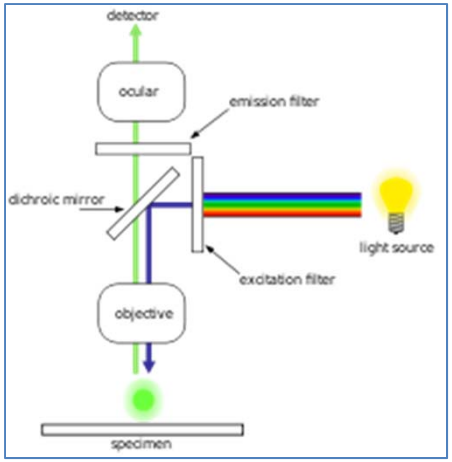

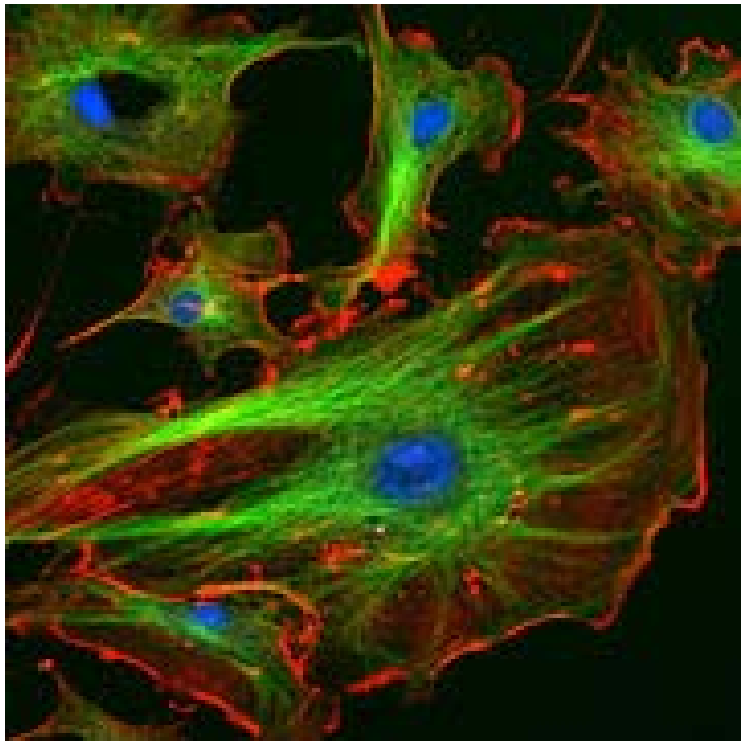

Endothelial cells under the microscope. Nuclei are stained blue with DAPI, microtubules are marked green by an antibody bound to FITC and actin filaments are labeled red with phalloidin bound to TRITC. Bovine pulmonary artery endothelial (BPAE) cells

The principle of confocal imaging was patented in 1957 by Marvin Minsky and aims to overcome some limitations of traditional wide-field fluorescence microscopes. In a conventional (i.e., wide-field) fluorescence microscope, the entire specimen is flooded evenly in light from a light source. All parts of the specimen in the optical path are excited at the same time and the resulting fluorescence is detected by the microscope's photodetector or camera including a large unfocused background part. In contrast, a confocal microscope uses point illumination and a pinhole in an optically conjugate plane in front of the detector to eliminate out-of-focus signal - the name "confocal" stems from this configuration. As only light produced by fluorescence very close to the focal plane can be detected, the image's optical resolution, particularly in the sample depth direction, is much better than that of wide-field microscopes. However, as much of the light from sample fluorescence is blocked at the pinhole, this increased resolution is at the cost of decreased signal intensity – so long exposures are often required.

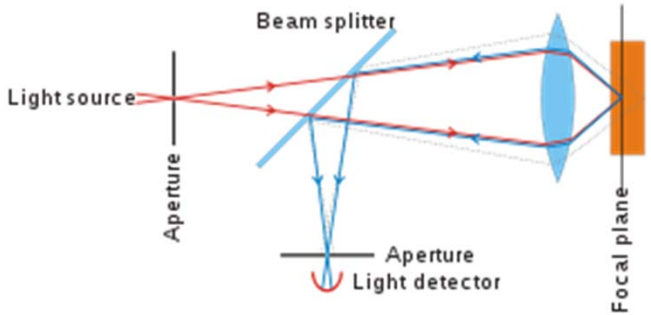

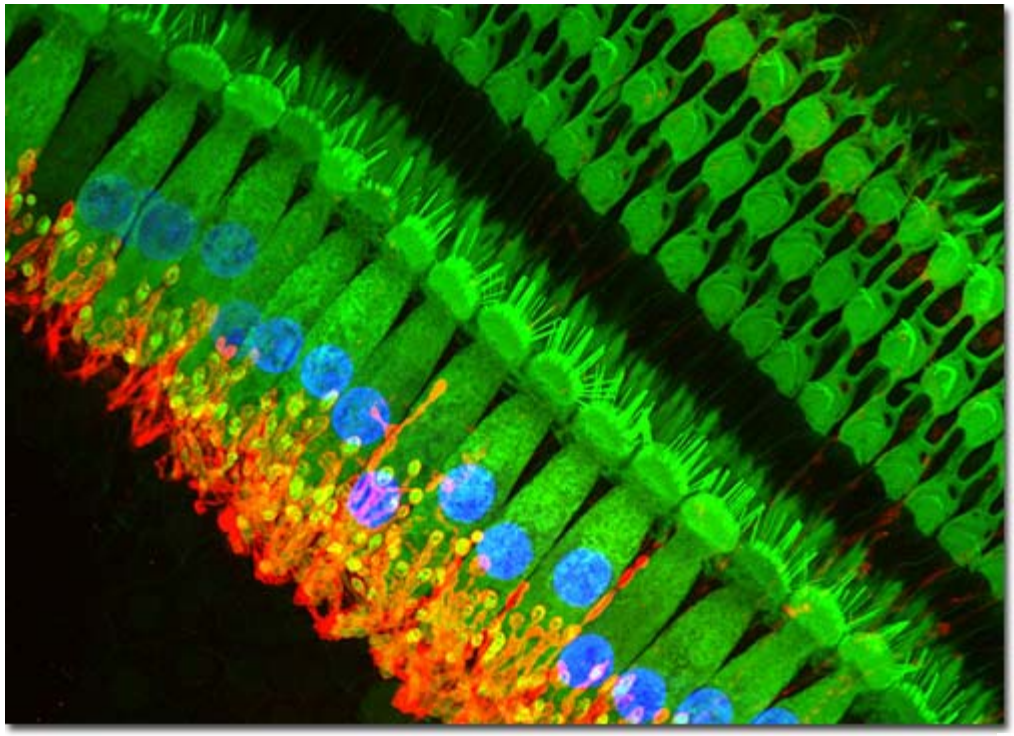

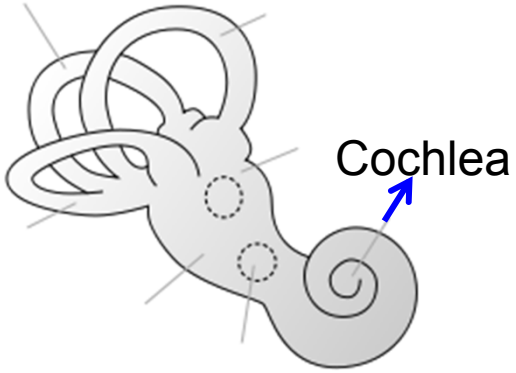

By Dr. Sonja Pyott
Department of Biology and Marine Biology
University of North Carolina, Wilmington
Wilmington, NC, USA
Specimen: Cochlea and Hair Cells
Technique: Confocal

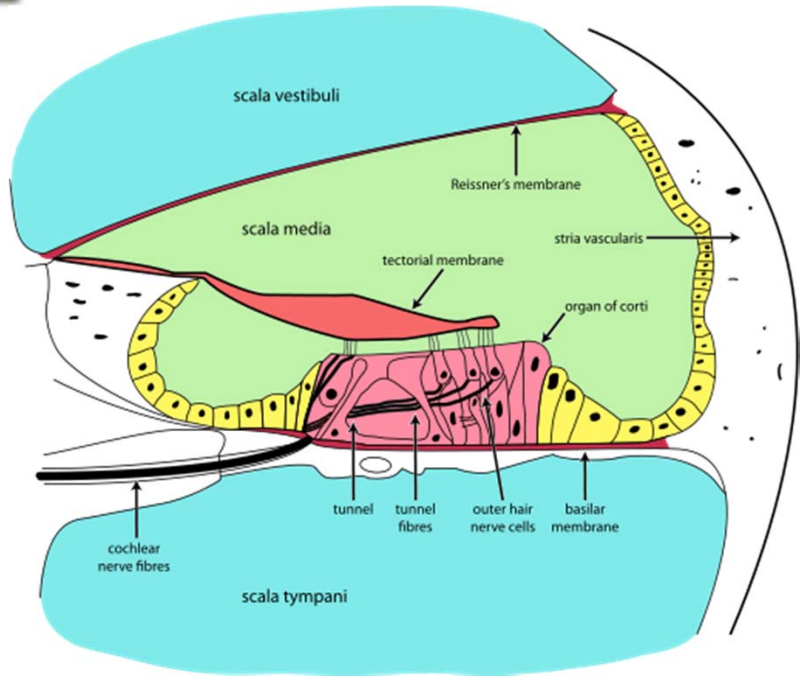

Lifetime imaging

FLIM is able to discriminate between fluorescence emanating from different fluorophores and autoflorescing molecules in a specimen, even if their emission spectra are similar. It is, therefore, ideal for identifying fluorophores in multi-label studies. FLIM can also be used to measure intracellular ion concentrations without extensive calibration procedures (for example, Calcium Green) and to obtain information about the local environment of a fluorophore based on changes in its lifetime. FLIM is often used to study spatial and temporal protein-protein interactions, properties of membranes and interactions with nucleic acids in living cells. FLIM is a key technique in enabling accurate FRET studies.

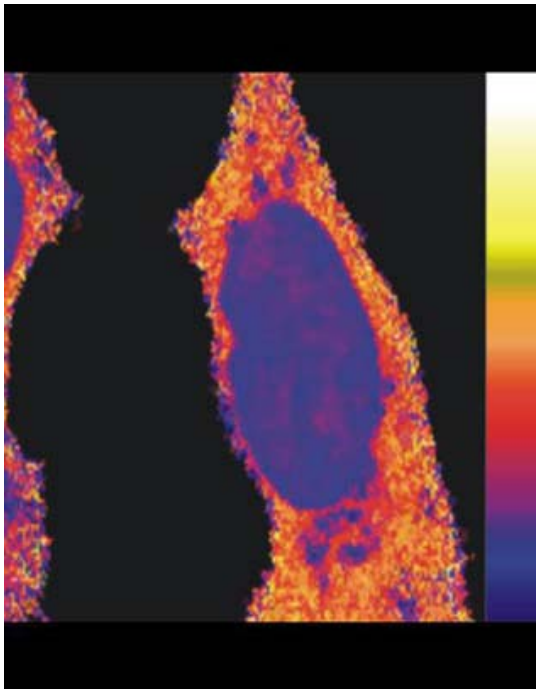

Superresolution microscopy

STORM, PALM and fPALM are super-resolution imaging techniques that utilize sequential activation and time-resolved localization of photoswitchable fluorophores to create high resolution images. During imaging, only an optically resolvable subset of fluorophores is activated to a fluorescent state at any given moment, such that the position of each fluorophore can be determined with high precision by finding the centroid position of the single-molecule images of particular fluorophore. The fluorophore is subsequently deactivated, and another subset is activated and imaged. Iteration of this process allows numerous fluorophores to be localized and a super-resolution image to be constructed from the image data.

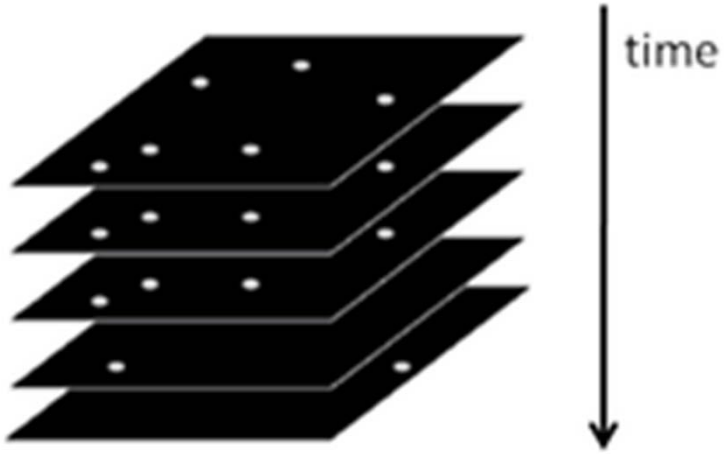

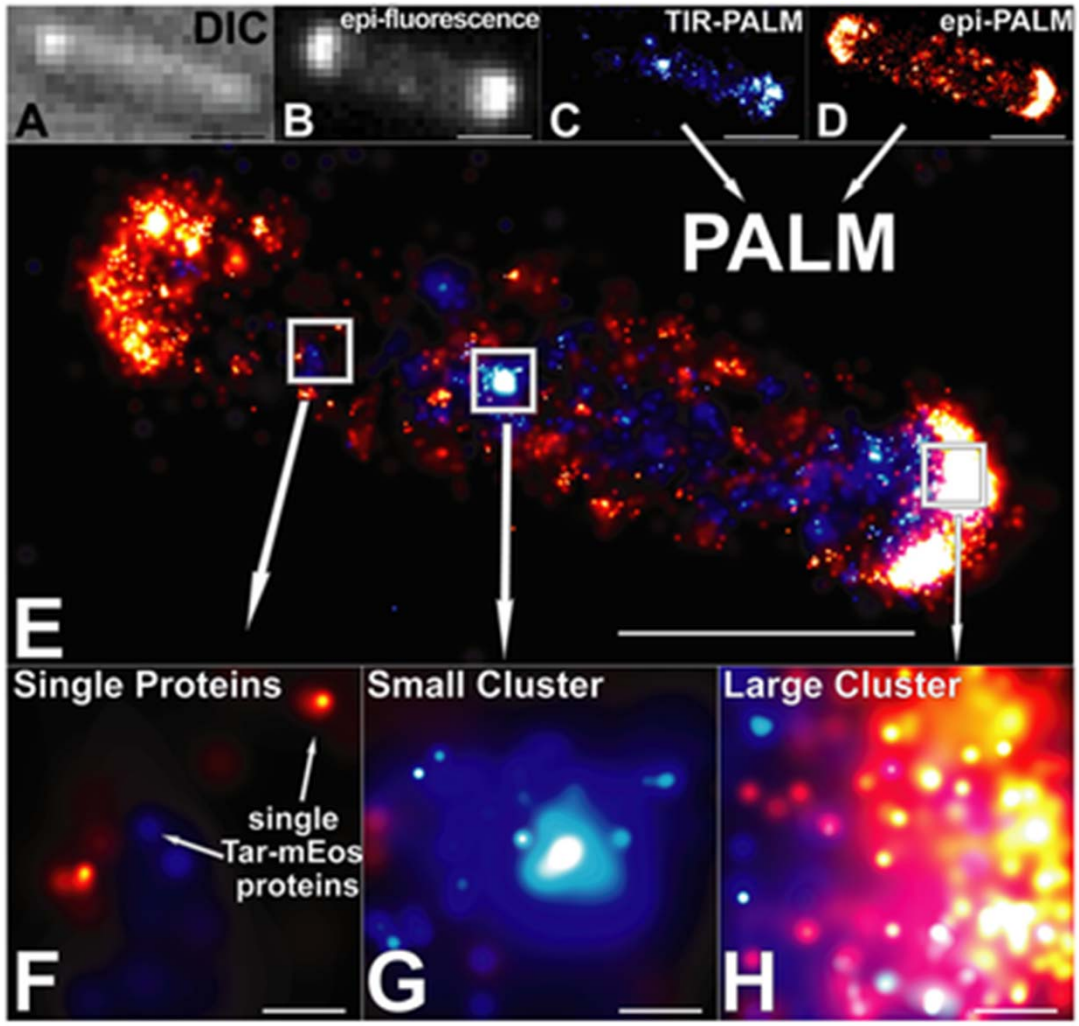

Self-organization of the escherichia coli chemotaxis network imaged with super-resolution light microscopy. Scale bar in (A–E) indicates 1 μm. Scale bar in (F–H) indicates 50 nm

SHG

Crystal materials lacking inversion symmetry can exhibit a so-called $\chi^{(2)}$ nonlinearity (→ *nonlinear crystal materials*). This can give rise to the phenomenon of frequency doubling [1], where an input (pump) wave generates another wave with twice the optical frequency (i.e. half the wavelength) in the medium. This process is also called *second-harmonic generation*. In most cases, the pump wave is delivered in the form of a laser beam, and the frequency-doubled (second-harmonic) wave is generated in the form of a beam propagating in a similar direction.

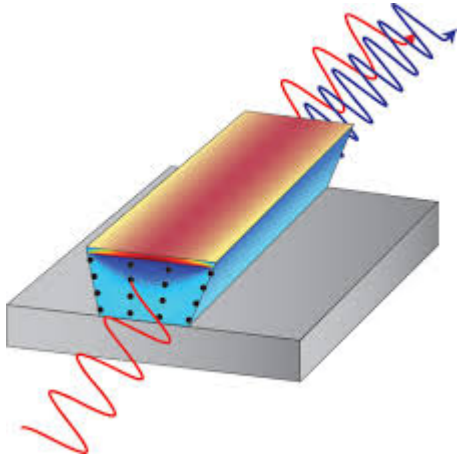

http://www.rp-photonics.com/frequency_doubling.html

Nonlinear microscopy

Second-harmonic imaging microscopy (SHIM) is based on a nonlinear optical effect known as second-harmonic generation (SHG). SHIM has been established as a viable microscope imaging contrast mechanism for visualization of cell and tissue structure and function. A second-harmonic microscope obtains contrasts from variations in a specimen's ability to generate second-harmonic light from the incident light while a conventional optical microscope obtains its contrast by detecting variations in optical density, path length, or refractive index of the specimen. SHG requires intense laser light passing through a material with a noncentrosymmetric molecular structure. Second-harmonic light emerging from an SHG material is exactly half the wavelength (frequency doubled) of the light entering the material.

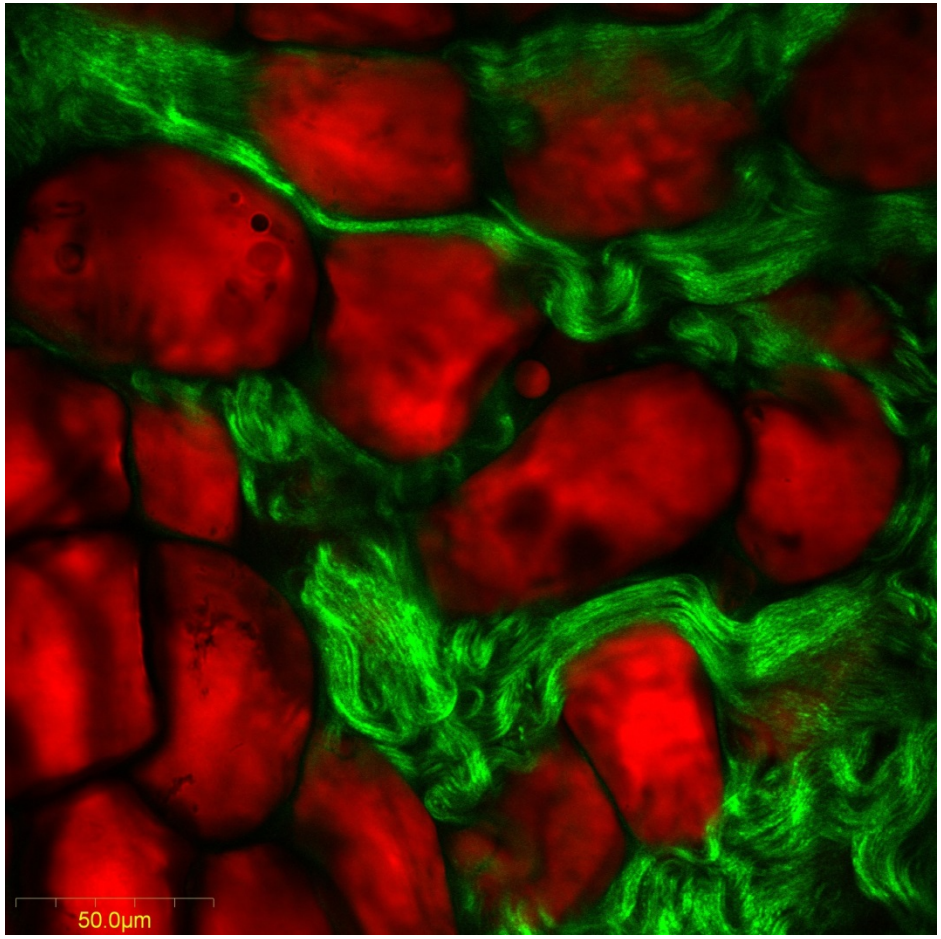

Red - several fat cells and in green with SHG microscopy collagen fibers

Optical imaging group - Twente University's Department of Science and Technology